RSC Advances

PAPER

View Article Online
View Journal | View Issue

Cite this: *RSC Adv.*, 2018, **8**, 38124

Amino-modified molecular sieves for adsorptive removal of H_2S from natural gas

Jiaojing Zhang,[ab] Hua Song,*[ab] Yanguang Chen,[ab] Tianzhen Hao,[c] Feng Li,[ab] Dandan Yuan,[ab] Xueqin Wang,[ab] Liang Zhao[d] and Jinsen Gao*[d]

Amine-modified MCM-41 adsorbents (APTMS/MCM-41, PEI/MCM-41 and AAPTS/MCM-41) were prepared and characterized by XRD, N_2 adsorption–desorption, FT-IR, TEM, SEM and TG-DTA. The performance of each adsorbent in a fixed adsorption bed for H_2S removal was measured using a mixture of oxygen, nitrogen and hydrogen sulfide gases. It was found that the specific surface area decreased and the topography changed significantly after the use of each modified adsorbent. Nevertheless, all amine-modified MCM-41 adsorbents retained mesoporous silica of MCM-41. The H_2S removal rate and saturated H_2S capacity of APTMS/MCM-41 improved from 32.3% to 54.2% and 119.5 to 134.4 mg g^{-1}, respectively, compared with that of MCM-41, and it showed the best performance among all adsorbents. APTMS/MCM-41, PEI/MCM-41 and AAPTS/MCM-41 were regenerated by maintaining at 423, 523 and 373 K in nitrogen for 3 h, respectively, and thus possessed high regenerability.

Received 16th August 2018
Accepted 25th October 2018

DOI: 10.1039/c8ra06859c

rsc.li/rsc-advances

Introduction

Hydrogen sulfide (H_2S) is frequently found in natural gas and other industrial hydrocarbon feedstocks. Since H_2S is one of the most noxious industrial gases to the atmosphere, the H_2S content of natural gas before use must be minimized to ensure no harm to human life and daily living.[1] Nowadays, alcohol amine solution is commonly used in industrial H_2S capture, and this method actually removes H_2S gas through a chemical reaction.[2] It utilizes the reaction between alcohol amines and H_2S to capture H_2S and the reverse reaction to regenerate the absorbent; this is the most efficient method for H_2S removal.[3] However, the disadvantages of this method for industrial applications include high energy consumption, large equipment volume, and significant equipment corrosion.[4] More researchers are investigating a more effective desulphurizing method. Solid adsorbents such as zeolites, activated carbon and molecular sieves have received much attention because the operations are simpler and less energy-consuming.[5] Research in the last few years has been focused on metal oxide-based adsorbents for efficient H_2S removal.[6–8] Many transition metals such as iron, copper and magnesium have been studied to load in carriers to improve the desulfurization capability of adsorbents.[9] However, the regeneration of adsorbents depends on high temperature, which restricts the application of solid adsorbents. Compared to existing absorption technologies based on amine solutions, amine-containing solid adsorbents are remarkable with less corrosiveness, amine loss and energy demand during the regeneration.[10,11] Among these solid supports, mesostructured MCM-41 is commonly used because of its high surface area, tuneable pore diameter and large pore volume.[12–17]

In the present study, APTMS/MCM-41, PEI/MCM-41 and AAPTS/MCM-41 were prepared, and their adsorptive desulfurization performances toward a simulated low-H_2S gas were studied. By comparing the loading with that of other amines, we directly attached certain amines to the carrier surfaces, but a chemical reaction occurred between some amines and the carrier to form a more stable material.

Experimental

Preparation of APTMS/MCM-41

Quantitatively calcined MCM-41 (all-silicon, Nankai University Catalyst Factory) was suspended in 30 mL of toluene (>99.5%, Nanjing Chemical Reagent Co., LTD) in a round-bottomed flask, into which 0.6 mL of (3-aminopropyl)trimethoxysilane (APTMS; >97%, Aladdin Reagent (Shanghai) Co., LTD) was cautiously added dropwise. After refluxing for 8 h, the resulting mixed solution was centrifuged to separate the target product from the solvent. The target product was then filtrated carefully first with ethanol and then distilled water; finally, it was dried at room temperature for 12 h.

Preparation of PEI/MCM-41

Quantitative polyethylenimine (PEI; >99%, Aladdin Reagent (Shanghai)) was completely dissolved in isopropyl alcohol

[a]Provincial Key Laboratory of Oil & Gas Chemical Technology, College of Chemistry & Chemical Engineering, Northeast Petroleum University, 163318 Daqing, China
[b]Key Laboratory of Enhanced Oil & Gas Recovery of Education Ministry, College of Petroleum Engineering, Northeast Petroleum University, 163318 Daqing, China
[c]Hebei Jingzhi Technology Co., LTD, 061000 Cangzhou, China
[d]State Key Laboratory of Heavy Oil Processing, China University of Petroleum (Beijing), 102249 Beijing, China. E-mail: jsgao@cup.edu.cn

(99.7%, Fu Chen (Tianjin) Chemical Reagent Factory). Then, 0.4 g of MCM-41 was added to the mixed solution, and the solution was stirred with a magnetic stirrer for some time. The resulting solution was filtered in a drying oven at 100 °C and dried for 4 h.

Preparation of AAPTS/MCM-41

Quantitatively calcined MCM-41 was suspended in 30 mL of toluene in a round-bottomed flask, into which 5 mL of *N*-ethyl-γ-amino propyl trimethoxy silane (AAPTS; 99.7%, Aladdin Shanghai) was cautiously added dropwise under a nitrogen atmosphere. After refluxing for 6 h, the resulting solution was centrifuged to separate the target product from the solvent. The product was filtrated carefully with distilled water and then dried at 100 °C for 12 h.

Characterization of adsorbent

The low-angle XRD patterns of all adsorbents were recorded on a Netherlands Panalytical diffractometer at 40 kV and 30 mA using monochromatized Cu-Kα radiation. The patterns were measured in the range of $2\theta = 0.5$–10°.

Physicochemical properties of the adsorbent and support were characterized on a NOVA2000e device (Quantachrome Instruments, USA). Each adsorbent was outgassed at 180 °C up to the vacuum pressure of 6 mmHg. The liquid nitrogen adsorption isotherms were monitored at −196 °C. Using the equation at a relative pressure (p/p_0) of 0.05–0.35, the Brunauer–Emmett–Teller (BET) surface area of each adsorbent was estimated from the adsorption isotherm. Total pore volume (V_{total}) was computed from the nitrogen volume at $p/p_0 = 0.99$.

The adsorbents were analyzed on a Bruker Tensor 27 Fourier transform infrared spectroscopy (FT-IR) spectrometer at room temperature. In advance, the adsorbents were mixed with dried KBr powder and tableted.

Morphology was analyzed on a JEOL 100S transmission electron microscope (TEM) was obtained on a JEOL 2010 microscope. For both TEM analyses, each adsorbent was prepared by adding a reduced sample (1 mg) to methanol (5 mL) and sonicated for 10 min. Several drops of suspension were added dropwise onto a hollow copper grid coated with a self-made carbon film.

Scanning electron microscopy (SEM) images were recorded on SIGMA SEM (Carl Zeiss AG, Germany) in vacuum at an accelerating voltage from 100 V to 30 kV to enlarge the sample by 2000–10 000 times.

The thermogravimetric-differential thermal analysis (TG-DTA) was recorded using a Perkin-Elmer Diamond thermal analyzer under atmospheric conditions and a temperature rate of 10 °C min^{-1}.

Desulfurization performance tests

Adsorbent activity measurements were conducted in a fixed-bed reactor. The fixed-bed reactor, which consisted of a quartz glass tube with 10 mm internal diameter and 300 mm length, was placed vertically in a clamshell furnace. The prepared adsorbent (0.2 g) was loaded into the center region of the reactor. The upper and lower sides of the adsorbent were filled with quartz sand. The model fuel gas (H_2S, N_2 and O_2 mixture; N_2 as balance gas; the H_2S concentration was controlled at about 20 mg L^{-1}) from a feed tank was passed through a reducing valve and entered into the reactor at a flow rate of 20 mL min^{-1}. Any unadsorbed H_2S gas in the effluent gas was dissolved by (the solvent of zinc acetate, cadmium acetate and acetic acid) in the absorption bottle, and the H_2S content in (the solvent of zinc acetate, cadmium acetate and acetic acid) was determined using iodometry at intervals of 5 min. The saturated H_2S capacity and H_2S removal rate of the absorbent were calculated using the H_2S breakthrough curves.

The saturated H_2S capacity is defined as the amount of adsorbed H_2S per gram of adsorbent when the H_2S concentrations in the effluent and in the initial gas are the same. It can be calculated as follows:

$$q_m = \frac{V \times \omega_{H_2S} - \left(c_{I_2} v_{I_2} - 0.5 c_{Na_2S_2O_3} v_{Na_2S_2O_3}\right) \times 34}{m} \quad (1)$$

Here, q_m is the saturated H_2S capacity (mg g^{-1}), ω_{H_2S} is the H_2S concentration in the sample gas (mg L^{-1}), V is the total gas volume (L), c_{I_2} is the concentration of I_2 (mol L^{-1}), v_{I_2} is the volume of I_2 (L), $c_{Na_2S_2O_3}$ is the concentration of $Na_2S_2O_3$ (mol L^{-1}), $v_{Na_2S_2O_3}$ is the volume of $Na_2S_2O_3$ (L), m is the amount of adsorbent (g), and 34 is the molar mass of H_2S (g mol^{-1}).

The H_2S removal rate (η) can be expressed as follows:

$$\eta = \frac{V \times \omega_{H_2S} - (c_{I_2} v_{I_2} - 0.5 c_{Na_2S_2O_3} v_{Na_2S_2O_3}) \times 34}{V \times \omega_{H_2S}} \times 100\% \quad (2)$$

Results and discussion

Low-angle XRD patterns of the four adsorbents are shown in Fig. 1. All adsorbents have one characteristic peak at $2\theta = 2.2^{\circ}$, which is ascribed to the (100) plane; the three weaker peaks correspond to the reflections of planes (110) at 3.8°, (200) at 4.4° and (210) at 5.7°, which are characteristics of the hexagonal mesoporous structure (Fig. 1).[18,19] The peak corresponding to the (100) plane could be considered as a feature of the MCM-41 mesostructure, indicating that the hexagonal mesoporous structure of MCM-41 was preserved after being loaded with APTMS, PEI or AAPTS. However, the (100) plane of the modified MCM-41 adsorbents was weaker compared with that of bare MCM-41, and even the peaks of other planes disappeared. As reported, the amine coating outside MCM-41 crystals did not significantly affect the diffraction intensity of MCM-41.[20,21] It is suggested that fast pore filling during amine modification is due to the smaller molecule size of amine. As more molecules entered pores during modification, structures collapsed rapidly and thereby reduced the diffraction intensity.[22–24]

Fig. 2 shows the N_2 adsorption–desorption isotherms and Barrett–Joyner–Halenda (BJH) pore size distributions for the four adsorbents and Table 1 lists their textural data. The isotherms belong to type IV according to the International Union of Pure and Applied Chemistry (IUPAC) classification, and they never varied after the loading of amine (APTMS, PEI or

AAPTS); this indicated that the organized network of MCM-41 was preserved after loading, which was in accordance with the XRD results (Fig. 1).[25,26] The H_1 type hysteresis loop at $p/p_0 > 0.9$ was due to N_2 condensation and evaporation with interparticles.[27,28] The nitrogen adsorption linearly increased at low relative pressures due to monolayer adsorption before the steep nitrogen uptake in the mesopores. Accordingly, micropore filling occurred at a low relative pressure, whereas sharp pore condensation was observed at a high pressure in the extended multilayer zone. The steep gas uptake was due to capillary condensation of nitrogen in the mesopores, implying that MCM-41 had a narrow pore size distribution. These results are consistent with the XRD patterns.

The BJH pore sizes of MCM-41 adsorbents (Fig. 2) were in the range of 2–6 nm, indicating that each adsorbent has excellent mesoporous ordering and a narrow pore size distribution. Bare MCM-41 exhibited a large specific surface area of 1095.2 $m^2\ g^{-1}$ and a pore volume up to 1.22 mL g^{-1}. The loading of APTMS, PEI or AAPTS changed the Brunauer–Emmett–Teller (BET) specific surface area, pore diameter and pore volume. The specific surface area and pore diameter significantly decreased with further increase in amine content. The external surface was saturated and more amines entered the mesopores of MCM-41, which caused pore blockage and therefore decreased the surface area.[25] These results were evidenced by the decrease in pore size with loading amine content. The specific surface area of PEI/MCM-41 was larger than those of APTMS/MCM-41 and AAPTS/MCM-41. This finding was possibly because PEI having a larger molecular size could not easily enter the inner pores of MCM-41 to be loaded on the internal surface of MCM-41; therefore, the loss in the surface area was less serious. The specific surface area of AAPTS/MCM-41 was the smallest possibly because the molecular size of AAPTS was smaller than that of PEI; therefore, it could easily enter the inner pores of MCM-41 as compared to PEI. In addition, the molecular size was larger than that of APTMS; therefore, the effect of AAPTS on the pore volume and surface area was more significant.

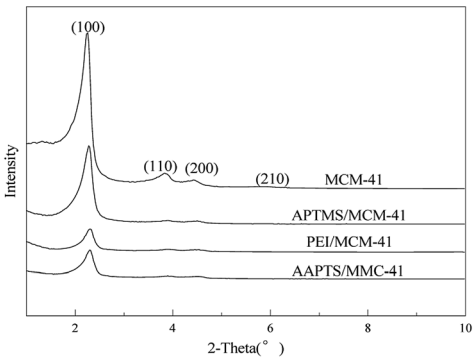

Fig. 1 Low-angle XRD patterns of MCM-41, APTMS/MCM-41, PEI/MCM-41 and AAPTS/MCM-41.

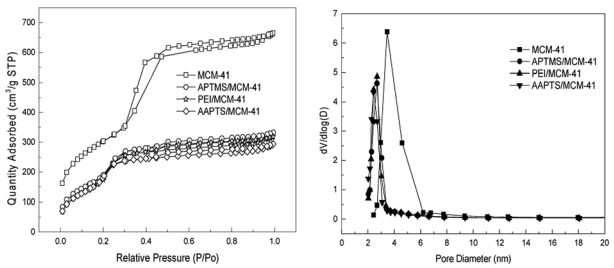

Fig. 2 Nitrogen adsorption–desorption isotherms and BJH pore size distribution curves of MCM-41, APTMS/MCM-41, PEI/MCM-41 and AAPTS/MCM-41.

The FT-IR spectra of the four adsorbents are shown in Fig. 3. The symmetrical stretching mode near 791 cm^{-1} and the asymmetric mode near 1076 cm^{-1} are related to the framework of silicon for the vibration of Si–O–Si. The adsorption bands at 3429 and 1632 cm^{-1} observed in all spectra are ascribed to the –OH stretching of silanol groups.[26,27] NH_2-MCM-41 shows a typical peak at 2939 cm^{-1} corresponding to the asymmetric vibration of $-CH_2$ in the propyl chain of the silylating agent.[28] The peaks of APTMS/MCM-41, PEI/MCM-41 and AAPTS/MCM-41 at 1532, 1463 and 1469 cm^{-1} (Fig. 3) correspond to the stretching vibration of C–N in the amine, which is specific to APTMS, PEI and AAPTS.[29] These results further confirm the successful immobilization of APTMS, PEI or AAPTS onto the surface of MCM-41.

The TEM image of MCM-41 shows the very rational and orderly channels on surface (Fig. 4a), revealing a uniform ordered hexagonal structure and a distinctive feature with pore diameter of ~4 nm. APTMS, PEI and AAPTS particles are uniformly distributed in the corresponding adsorbent (Fig. 4b–d) and thus are highly dispersed. The APTMS, PEI and AAPTS particles appear either on the external surface walls of the pores or inside the pores, indicating strong interactions between organic amine and MCM-41.

The SEM images of the four adsorbents show various particle shapes and sizes (Fig. 5). The micrographs show that the coupling agent APTMS, PEI or AAPTS influences the microstructure of MCM-41 to a greater extent. The SEM images show that the surface of MCM-41 is relatively smooth with different sizes and relatively sparse channels (Fig. 5a). However, the SEM images of APTMS/MCM-41 show greater changes on the

Table 1 Surface property of MCM-41, APTMS/MCM-41, PEI/MCM-41 and AAPTS/MCM-41

Adsorbents	Surface area/($m^2\ g^{-1}$)	Pore diameter/nm	Pore volume/(mL g^{-1})
MCM-41	1095.2	3.64	1.22
APTMS/MCM-41	873.7	2.89	0.64
PEI/MCM-41	882.2	2.80	0.70
AAPTS/MCM-41	823.9	2.80	0.60

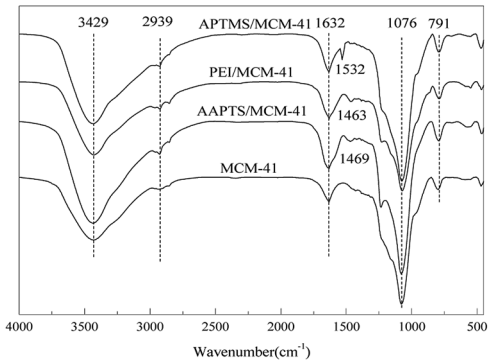

Fig. 3 FT-IR spectra of MCM-41, APTMS/MCM-41, PEI/MCM-41 and AAPTS/MCM-41.

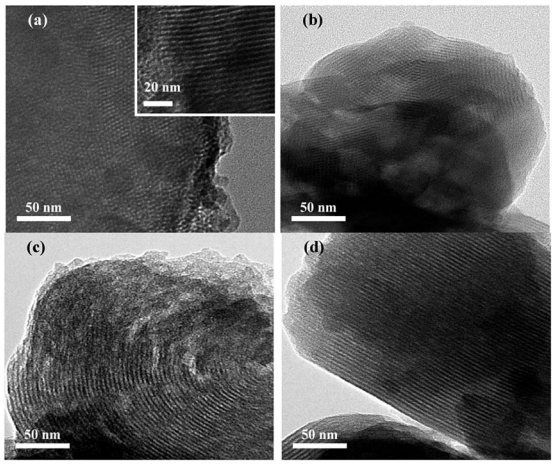

Fig. 4 TEM images of MCM-41 (a), APTMS/MCM-41 (b), PEI/MCM-41 (c) and AAPTS/MCM-41 (d).

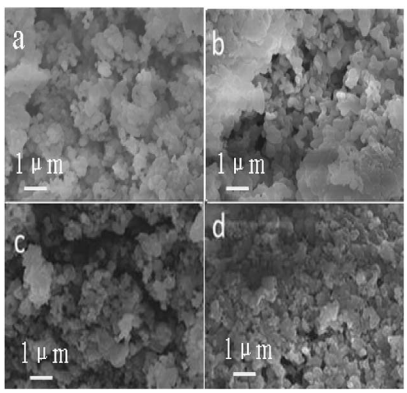

Fig. 5 SEM images of MCM-41 (a), APTMS/MCM-41 (b), PEI/MCM-41 (c) and AAPTS/MCM-41 (d).

surfaces. The APTMS/MCM-41 particles are worm-like. The particles are well ordered and arranged in the best way for amine loading (Fig. 5b).[30] PEI distributes unevenly on MCM-41 pores and clogs parts when it is loaded on MCM-41 (Fig. 5c). The active constituent in AAPTS/MCM-41 distributes much more evenly than in PEI/MCM-41, indicating that the existence of

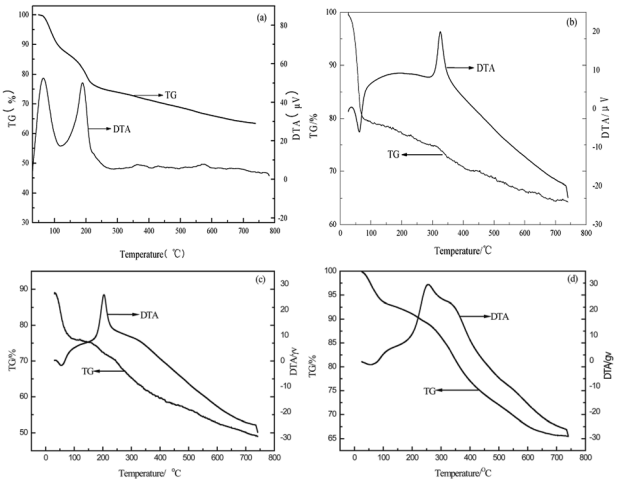

Fig. 6 TG-DTA curves of MCM-41 (a), APTMS/MCM-41 (b), PEI/MCM-41 (c) and AAPTS/MCM-41 (d).

AAPTS is propitious to the dispersion of the active component. The surface channel distribution of modified MCM-41 is dense; the holes are filled with the active component, and pore formation is completed during loading although the surface area decreases with smaller pore volumes. These results are consistent with BET data.

The TG-DTA curves of the four adsorbents are shown in Fig. 6. MCM-41 displays one stage of weight loss with an endothermic peak within 50–200 °C (22.3%), whereas APTMS/MCM-41, PEI/MCM-41 and AAPTS/MCM-41 show one stage of weight loss at endothermic peaks within the ranges of 25–70 °C (19.2%), 30–93 °C (23.7%), 25–85 °C (5.5%), respectively. These findings can be ascribed mainly to water elimination from the surface and pores. Other exothermic peaks at 326, 204 and 256 °C are owing to $-NH_2$ decomposition of APTMS/MCM-41, PEI/MCM-41 and AAPTS/MCM-41, respectively. In addition, the different features from the TG/DTA curves of the four adsorbents, which show a greater mass loss for pure MCM-41 than that for modified MCM-41 adsorbents, may indicate interaction between the incorporated amine component and the surfactant molecules. Thus, the stability of MCM-41 is improved.[31] The decomposition temperature of $-NH_2$ decreases in the order APTMS/MCM-41 > AAPTS/MCM-41 > PEI/MCM-41. This shows that APTMS/MCM-41 has the highest stability. This result is consistent with the order of the molecular size of loaded molecules, which indicates that smaller molecules are more stable.

All adsorbents were evaluated at room temperature (298.15 K) and gas speed of 20 mL min^{-1} in a fixed-bed reactor (Fig. 7 and Table 2). The H_2S removal performances of the adsorbents improved significantly after amine modification, which proves that the presence of organic amine is critical in H_2S removal. The saturated H_2S capacities decreased in the order APTMS/MCM-41 > AAPTS/MCM-41 > PEI/MCM-41 > MCM-41, with 134.4, 46.6, 40.2 and 14.9 mg g^{-1}, respectively. For APTMS/MCM-41, the desulfurization performance with saturated adsorption at 186 min was higher than that of all the modified adsorbents. The saturated H_2S capacity and H_2S removal rate maximized to 134.38 mg g^{-1} and 54.19%, respectively, at the

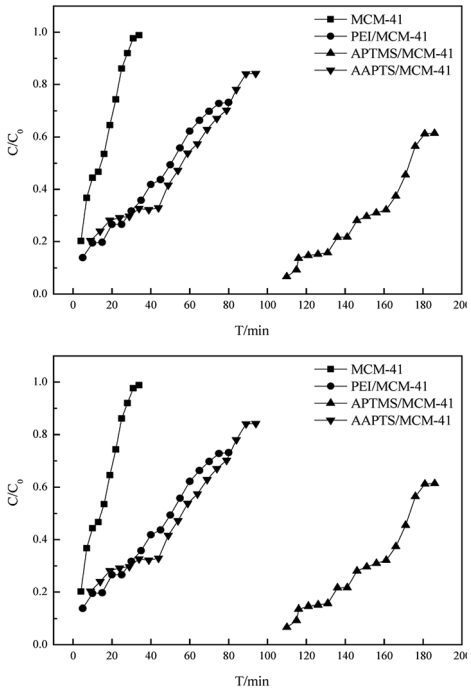

Fig. 7 Breakthrough curves of MCM-41, APTMS/MCM-41, PEI/MCM-41 and AAPTS/MCM-41.

APTMS loading of 1 g. The higher saturated H_2S capacity and H_2S removal obtained by APTMS/MCM-41 could be explained as follows: the molecular size of the loaded molecule increased in the order of APTMS < AAPTS < PEI (Fig. 8). APTMS with small size could easily enter the inner pores of MCM-41 and react with –OH on the inner pore surface of MCM-41. As a result, APTMS/MCM-41 possessed many active sites compared to PEI/MCM-41 and AAPTS/MCM-41. In addition, as compared to the results for AAPTS/MCM-41, the FT-IR spectra of APTMS/MCM-41 showed a greater stretching vibration peak for C–N in the amine around 1532 cm^{-1} (Fig. 3). This may clearly indicate that APTMS/MCM-41 has high alkalinity, which can lead to more active sites.[32] In conclusion, saturated H_2S capacity and H_2S removal obtained by APTMS/MCM-41 were much higher than those of PEI/MCM-41 and AAPTS/MCM-41. As compared to PEI, AAPTS possessed a much smaller molecular size; however, the saturated H_2S capacity and H_2S removal rate were just slightly higher than that of PEI/MCM-41. This can be explained by the much lower surface area of AAPTS/MCM-41 as compared to that of PEI/MCM-41 (Table 1).

Regeneration experiments in a fixed-bed reactor showed that regeneration of APTMS/MCM-41, PEI/MCM-41 and AAPTS/MCM-41 was achieved by maintaining at 423, 523 and 373 K in nitrogen for 3 h, respectively. The breakthrough curves of APTMS/MCM-41, PEI/MCM-41 and AAPTS/MCM-41 after regeneration time of 3 h are shown in Fig. 9 and Table 3. The saturated H_2S capacities after regeneration time of 3 h decreased in the order APTMS/MCM-41 > AAPTS/MCM-41 > PEI/MCM-41, with the calculated values of 103.6, 32.5 and 27.3 mg g^{-1}, respectively. The recovered saturated H_2S capacities of APTMS/MCM-41, PEI/MCM-41 and AAPTS/MCM-41 after regeneration time of 3 h were still much higher than that of MCM-41, indicating high regenerability of the amine-modified MCM-41 adsorbents.

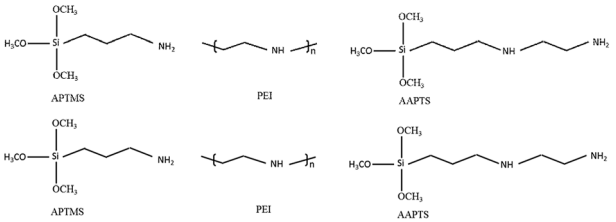

Fig. 8 Molecular structure formula of APTMS, PEI and AAPTS.

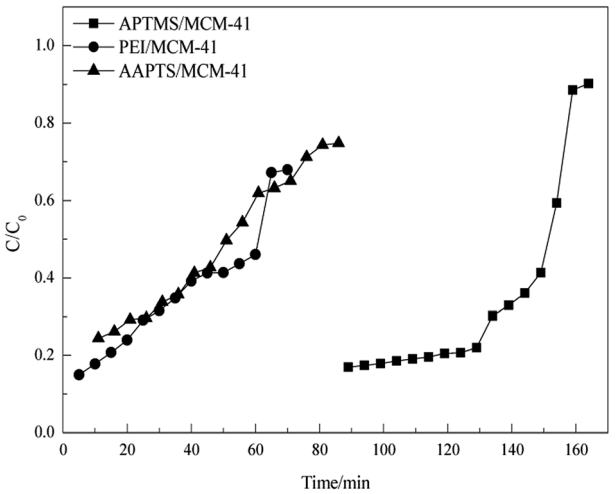

Fig. 9 Breakthrough curves of APTMS/MCM-41, PEI/MCM-41 and AAPTS/MCM-41 adsorbents after regeneration time of 3 h.

The adsorption mechanism of desulfurization can be described by the following steps:[33–35] (1) H_2S molecules diffuse to the external surface of the adsorbent from the bulk of gas; (2) H_2S molecules diffuse from the external surface to the inside of the pores; (3) a chemical adsorptive desulfurization reaction

Table 2 Desulfurization performance of MCM-41, APTMS/MCM-41, PEI/MCM-41 and AAPTS/MCM-41

Adsorbents	Saturated adsorption time/min	Saturated H_2S capacity/(mg g^{-1})	H_2S removal rate/%
MCM−41	34	14.9	21.9
APTMS/MCM−41	186	134.4	54.2
PEI/MCM−41	80	40.2	42.1
AAPTS/MCM−41	94	46.6	44.8

Table 3 Desulfurization performance of APTMS/MCM-41, PEI/MCM-41 and AAPTS/MCM-41 adsorbents after regeneration time of 3 h[a]

Adsorbents	Saturated adsorption time/min	Saturated H_2S capacity/(mg g^{-1})	H_2S removal rate/%
APTMS/MCM-41	164	103.6	51.2
PEI/MCM-41	70	27.3	36.7
AAPTS/MCM-41	86	32.5	38.8

[a] AAPTS/MCM-41 adsorbents after regeneration time of 3 h.

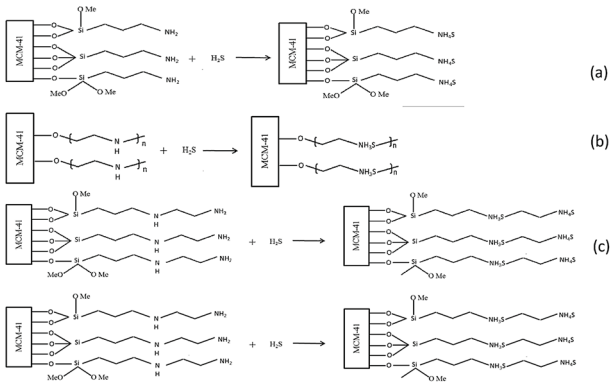

Scheme 1 Possible mechanism of APTMS/MCM-41 (a), PEI/MCM-41 (b) and AAPTS/MCM-41 (c) adsorbents.

occurs and results in the formation of a sulfur-containing organic compound; (4) complete sulfidation of the active phase and the absorbent leads to adsorption saturation. Some possible mechanisms underlying the trend of reactivity are illustrated in Scheme 1. The desorption process was the reverse reaction of adsorption, in which H_2S was released from adsorbent at a high temperature during regeneration.

Conclusions

Amine-modified MCM-41 adsorbents (APTMS/MCM-41, PEI/MCM-41 and AAPTS/MCM-41) were successfully prepared. XRD demonstrated that all amine-modified adsorbents retained mesoporous silica of MCM-41. The BET specific surface areas of the modified adsorbents decreased, and surface areas and pore size also decreased owing to the loading of APTMS, PEI and AAPTS in the pore canals of MCM-41. The fixed-bed adsorption desulfurization experiments showed that H_2S removal improved significantly after modification. The desulfurization performances decreased in the order APTMS/MCM-41 > AAPTS/MCM-41 > PEI/MCM-41 > MCM-41. The saturated adsorption time was 186 min with a total gas volume of 3720 mL, and the saturated H_2S capacity and H_2S removal rate maximized to 134.4 mg g^{-1} and 54.2%, respectively. Regeneration of APTMS/MCM-41, PEI/MCM-41 and AAPTS/MCM-41 was achieved by maintaining at 423, 523 and 373 K in nitrogen for 3 h, respectively. The recovered saturated H_2S capacities of APTMS/MCM-41, PEI/MCM-41 and AAPTS/MCM-41 after regeneration time of 3 h were still much higher than that of MCM-41, indicating high regenerability of amine-modified MCM-41 adsorbents.

Conflicts of interest

There are no conflicts to declare.

Acknowledgements

This research was supported by the Mentoring Project of China Petroleum, the Chemical Industry Federation (2016-09-27), and the Natural Science Foundation of Heilongjiang Province (QC2017005).

References

1 Y. Sun, X. W. Liu, W. Su, Y. Zhou and L. Zhou, *Appl. Surf. Sci.*, 2007, **253**, 5650–5655.
2 S. Moioli, A. Giuffrida, M. C. Romano, L. A. Pellegrini and G. Lozza, *Appl. Energy*, 2016, **183**, 1452–1470.
3 S. J. Majeed, *J. Nat. Gas Sci. Eng.*, 2016, **36**, 175–183.
4 M. Hamdine, M. C. Heuzey and A. Bégin, *Int. J. Biol. Macromol.*, 2005, **37**, 134–142.
5 M. Behl, J. Yeom, Q. Lineberry, P. K. Jain and M. A. Shannon, *Nat. Nanotechnol.*, 2012, **7**, 810–815.
6 M. M. Wu, L. Shi, W. Su, T. T. Lim, A. Vedsha, F. Yu, H. L. Fan and J. Mi, *Chem. Eng. J.*, 2018, **353**, 273–287.
7 M. M. Wu, T. Li, H. Yu. Li, H. L. Fan and J. Mi, *Energy Fuels*, 2017, **31**, 13921–13932.
8 M. M. Wu, B. W. Chang, T. T. Lim, W. D. Oh, J. X. Lei and J. Mi, *J. Hazard. Mater.*, 2018, **360**, 391–401.
9 Z. B. Huang, B. S. Liu, F. Wang and R. Amin, *Appl. Surf. Sci.*, 2015, **353**, 1–10.
10 Q. Chen, F. Fan, D. Long, X. Liu, X. Liang, W. Qiao, *et al.*, *Ind. Eng. Chem. Res.*, 2010, **49**, 11408–11414.
11 B. Yoosuk, T. Wongsanga and P. Prasassarakich, *Fuel*, 2016, **168**, 47–53.
12 A. S. Khder, H. Hma and M. S. Elshall, *Appl. Catal., A*, 2012, **411**, 77–86.
13 A. Marcilla, A. Gómez-Siurana, D. Berenguer, I. Martínez-Castellanos and M. I. Beltrán, *Toxicol. Rep.*, 2015, **2**, 152–164.
14 F. Farjadian, P. Ahmadpour, S. M. Samani and M. Hosseini, *Microporous Mesoporous Mater.*, 2015, **213**, 30–39.
15 M. Nikoorazm, A. Ghorbani-Choghamarani, H. Mahdavi and S. M. Esmaeili, *Microporous Mesoporous Mater.*, 2015, **211**, 174–181.
16 T. Yasmin and K. Müller, *Microporous Mesoporous Mater.*, 2015, **208**, 83–92.
17 T. Intana, K. Föttinger, G. Rupprechter and P. Kongkachuichay, *Colloids Surf., A*, 2015, **467**, 157–165.

18 P. Benito, M. Gregori, S. Andreoli, G. Fornasari, F. Ospitali, S. Millefanti, *et al.*, *Catal. Today*, 2015, **246**, 108–115.
19 D. Marino, N. G. Gallegos, J. F. Bengoa, A. M. Alvarez, M. V. Cagnoli, S. G. Casuscelli, E. R. Herrero and S. G. Marchetti, *Catal. Today*, 2008, **133–135**, 632–638.
20 M. F. Mota, A. C. L. PatrãCio, M. M. D. Silva and M. G. Freire Rodrigues, *Mater. Sci. Forum*, 2014, **805**, 667–671.
21 X. Xu, C. Song, J. M. Andresen, B. G. Miller and A. W. Scaroni, *Energy Fuels*, 2015, **16**, 1463–1469.
22 S. Huh, J. W. Wiench, J. C. Yoo, M. Pruski and V. S. Y. Lin, *Chem. Mater.*, 2003, **15**, 4247–4256.
23 M. M. da Silva, A. C. L. Patrício, A. K. F. de Sousa, M. G. Freire Rodrigues and M. L. P. da Silva, *Mater. Sci. Forum*, 2015, **805**, 657–661.
24 C. García-Sancho, R. Moreno-Tost, J. Mérida-Robles, J. Santamaría-González, A. Jiménez-López and P. Maireles-Torres, *Appl. Catal., A*, 2012, **433**, 179–187.
25 C. T. Kresge, M. E. Leonowicz, W. J. Roth, J. C. Vartuli and J. S. Beck, *Nature*, 1992, **359**, 710–712.
26 K. Parida, K. G. Mishra and S. K. Dash, *J. Hazard. Mater.*, 2012, **241**, 395–403.
27 X. Chen, X. L. Wang, G. Ran, Z. Cui, S. H. Chen and K. Xie, *Fine Chemicals*, 2016, **33**(2), 188–194.
28 H. Zhao, J. Hu, J. Wang, L. Zhou and H. Liu, *Acta Phys.-Chim. Sin.*, 2007, **23**, 801–806.
29 J. Cheriaa, M. Khaireddine, M. Rouabhia and A. Bakhrouf, *Sci. World J.*, 2012, **2012**, 512454.
30 K. S. N. Kamarudin and N. Alias, *Fuel Process. Technol.*, 2013, **106**, 332–337.
31 A. S. Khder, H. Hma and M. S. Elshall, *Appl. Catal., A*, 2012, **411**, 77–86.
32 A. Endo, M. Yamada, S. Kataoka, T. Sano, Y. Inagi and A. Miyaki, *Colloids Surf., A*, 2010, **357**, 11–16.
33 J. J. Zhang, L. Wang, H. Song and H. L. Song, *Res. Chem. Intermed.*, 2015, **41**, 6087–6104.
34 J. J. Zhang, G. J. Wang, W. Y. Wang, H. Song and F. S. Li, *Res. Chem. Intermed.*, 2016, **42**, 6003–6012.
35 D. T. Dixon, D. H. Herzog, D. S. Twinning, S. J. J. Titinchi, M. Piet, H. S. Abbo, O. Bolland and W. Schwieger, *Energy Procedia*, 2014, **63**, 8153–8160.